Parabolic polarization splitting of Tamm states in a metal-organic microcavity

R. Brückner,[1,a)] M. Sudzius,[1] S. I. Hintschich,[1] H. Fröb,[1] V. G. Lyssenko,[1] M. A. Kaliteevski,[2,3] I. Iorsh,[4] R. A. Abram,[4] A. V. Kavokin,[5] and K. Leo[1]
[1]*Institut für Angewandte Photophysik, Technische Universität Dresden, 01062 Dresden, Germany*
[2]*Ioffe Physicotechnical Institute, 194021 St. Petersburg, Russia*
[3]*St. Petersburg Academic University, 8/3 Khlopina, St. Petersburg, Russia*
[4]*Department of Physics, Durham University, Durham DH1 3LE, United Kingdom*
[5]*School of Physics and Astronomy, Southampton University, Southampton SO17 1BJ, United Kingdom*

(Received 18 October 2011; accepted 13 January 2012; published online 7 February 2012)

We observe hybrid states of cavity photons and Tamm plasmons in an organic microcavity with an incorporated thin silver layer of increasing thickness up to 40 nm. Via μ-photoluminescence spectroscopy, we investigate their angular dependence. At oblique angles, we observe a TE-TM polarization splitting of more than 40 meV for each mode. An analytical model is developed to describe the coupling of Tamm plasmons and cavity photons and to account for the splitting of the orthogonally polarized resonances. © *2012 American Institute of Physics*. [doi:10.1063/1.3681374]

The localization of light in a microcavity enables the observation of strong light-matter coupling in solid state devices and paves the way for demonstrating a wide range of fundamental effects such as Bose condensation of polaritons,[1–3] superfluidity,[4] vortex formation,[5] and multi-stability.[6,7] The observation of these phenomena has led to the development of concepts for a new class of optoelectronic devices like electrically pumped polariton light emitting diodes,[8,9] polariton processing circuits,[10] and spin-optronic devices.[11]

An important property of planar microcavities is the splitting of their resonances into different linear polarizations, usually referred to as TE-TM splitting. This, in turn, is responsible for various phenomena in the newly emerging field of spin-optronics, including the "all optical" spin Hall effect and the formation of polarized patterns. Recently, much attention has been paid to a study of the possible generation of optical states possessing non-zero orbital angular momentum, which could find applications in quantum information processing.[12]

Initially, microcavities were entirely realized with semiconductors, but recently it has been shown that the inclusion of metallic layers in a microcavity is interesting both for fundamental effects and applications: It was shown that the introduction of metallic components into a microcavity leads to the appearance of additional localized optical states, so called Tamm plasmons,[13] which can strongly couple to cavity polaritons.[14] In dielectric microcavities, metal layers can play numerous roles simultaneously: they lead to the appearance of Tamm plasmons and determine their eigenenergies and can be used to contact and control the properties of the device electrically.[15,16]

In this work, we study the coupling of various modes with different polarizations present in an organic microcavity with an incorporated thin silver layer (thickness up to 40 nm). The experimentally obtained parabolic dispersion relations $E(k)$ of hybrid states of a Tamm plasmon and a cavity mode is confirmed numerically and modeled analytically. The sample investigated is shown in Figure 1. It consists of a microcavity structure composed of two distributed Bragg reflectors (DBRs) with an embedded organic half-λ cavity layer made of the host-guest system tris-8-hydroxyquinoline aluminium (Alq3) doped with 2 wt. % of 4-dicyanomethylene-2-methyl-6-p-imethylaminostyryl-4 H-pyran (DCM). A silver layer with its thickness graded from 0 to 40 nm is deposited on top of the first DBR, enclosed by the active cavity layer and the top DBR. The optical thicknesses of both the cavity and the 21 alternating $\lambda/4$ layers of TiO_2/SiO_2 forming each DBR are chosen to correspond to the maximum of the DCM emission at ~630 nm. Due to the wedged shape, the silver layer only partly covers the first mirror resulting in a high quality, all-dielectric microcavity as well as a microcavity with varying metal thickness up to 40 nm, see also Ref. 17 for more details.

A μ-photoluminescence (μ-PL) microscope setup is utilized to investigate the angle-resolved emission spectra of our structure at room temperature. By focusing the beam of a

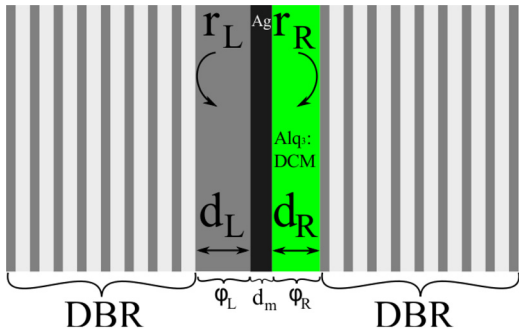

FIG. 1. (Color online) Design of the structure investigated. Two Bragg reflectors enclose the cavity layer and the silver layer of variable thickness (gradient from 0 to 40 nm). The reflection coefficients at the corresponding interfaces are marked as r_i, the thicknesses of the layers being most sensitive to the eigenmodes as d_i. The topmost TiO_2 layer of the first DBR ($i = L$), the silver ($i = m$) and cavity ($i = R$) layers are shown not to scale.

[a)]Author to whom correspondence should be addressed. Electronic mail: Robert.Brueckner@iapp.de.

405 nm cw laser with a microscope objective (× 25, NA 0.5) to a spot diameter of less than 2 μm, areas either with or without metal can be selectively excited. Such a small spot size is necessary in order to avoid collecting PL-signal from areas with different thickness of the silver layer resulting in different spectral features. The high aperture of the objective (×63, NA 0.8) collecting the sample emission covers a large angular range of around ± 55° in the far field geometry. A second lens is used to map the Fourier plane of the first collecting objective enabling the observation of the dependence $E(k)$. A polarization filter installed in front of the spectrometer is utilized to characterize the polarization properties of the sample emission. The spectrograph is equipped with a cooled charge-coupled device to record the spectrally, angularly, and polarization-resolved PL signal.

In Figure 2, the experimental angle-resolved emission spectra of the metal organic microcavity are shown for different metal thicknesses (left panels of Figs. 2(a)–2(d). These are compared to the results of numerical calculations based on the transfer matrix algorithm (right panels). Three phenomena become apparent: First, because of the graded thickness of the metal layer placed inside the cavity and the small excitation spot used, an increasing metal thickness means moving away from metal-free areas. Thus, any scatter of the emission into metal free areas is reduced, leading to a weaker coupling into the original cavity mode at 632 nm. This behavior is not accounted for in our numerical calculations, since we assume a constant metal thickness over large areas (compare left and right panels in Figs. 2(a)–2(d) at 632 nm). Next, depending on the metal thickness, two modes arise. The spectrally broad emission above 700 nm corresponds to emission into the long wavelength sideband of the DBRs. At silver thicknesses of ~25 nm, an initially broad mode emerges from the long wavelength sideband. This is a

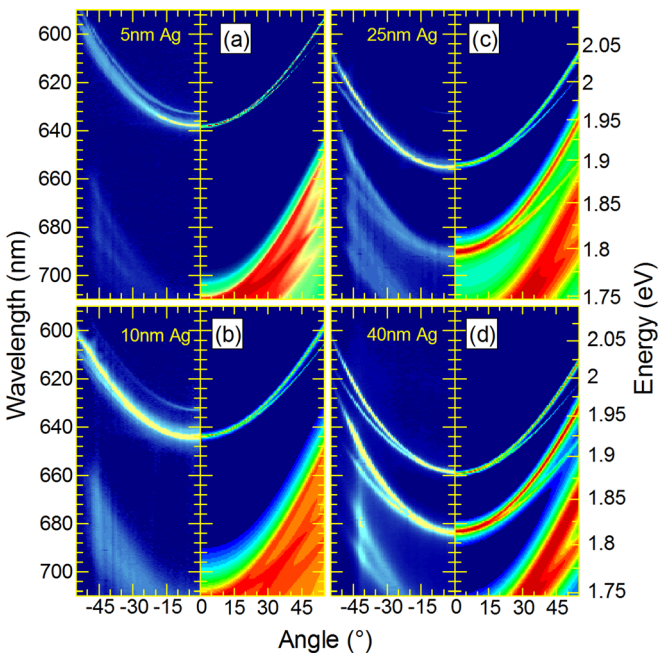

FIG. 2. (Color online) Experimentally observed angle-resolved emission spectra (left panels) along with numerically calculated spectra (right panels). Deviations of the shape of the parabolae are due to imperfect refractive indices and their dispersions, on which simulations are based.

so-called Tamm plasmon-polariton, which has its origin in the localization of the electromagnetic field next to the metal layer.[17] In addition to this, a high energy resonance is observed, which at zero metal thickness converges to the original cavity mode. As metal is introduced, it starts shifting to the red. The reason for this shift is the coupling of this mode to the Tamm plasmon-polariton evidenced by a clear anticrossing behavior of the involved modes. This was previously reported[17] and is further discussed later. Finally, at oblique angles and certain thicknesses of the embedded metal layer, a splitting of each mode is observed. Moreover, this splitting increases towards large angles of incidence. We observe that the polarizations of both branches are orthogonal to each other, characteristic of a splitting between TE- (lower branch) and TM-polarization (upper branch). With increasing metal thickness, the modes become increasingly detuned with respect to the center of the DBR stop bands. The degree of polarization splitting depends on any additional phase shift, such as for example, by a detuning of the resonant modes,[18–20] anisotropy of the organic[21] or inorganic structures,[22] and polarization dependent reflections at the metal surfaces. In our structure, the most sensitive way to control these phase shifts is by varying the thickness of the metal layer. In addition to the phase shift at the dielectric/metal interface, the reflectance and transmittance of this layer can be varied, which affects the coupling of the resonant modes. The observed splitting is strongly pronounced, reaching values of 37 meV for the shifted cavity mode and 45 meV for the Tamm plasmon-polariton state at angles of ±55° and a silver layer thickness of 40 nm.

In addition to numerical modeling, we have developed an analytical description of the system to gain a physical understanding of the eigenmodes of a coupled cavity photon mode and a Tamm plasmon. This is realized using a transfer matrix algorithm for complex amplitudes to describe electromagnetic waves propagating forward and backward at both interfaces of the left and right DBR (see Figure 1)

$$A\begin{pmatrix}1\\ r_R\end{pmatrix}=\begin{pmatrix}e^{i\varphi_L} & 0\\ 0 & e^{-i\varphi_L}\end{pmatrix}\begin{pmatrix}(t^2-r^2) & r\\ -r & 1\end{pmatrix}\times\begin{pmatrix}e^{i\varphi_R} & 0\\ 0 & e^{-i\varphi_R}\end{pmatrix}\begin{pmatrix}r_L\\ 1\end{pmatrix}. \quad (1)$$

Here, the amplitude reflection coefficient of the left (right) DBR is $r_{L(R)}$, the amplitude transmission and reflection coefficients of the silver layer are t and r. The phase shifts occurring due to the propagation through layers adjacent to silver are given by $\varphi_i = n_i d_i \cos\Theta_i(\omega/c)$, with the angle of light propagation relative to the normal of the interfaces Θ_i, the thickness d_i, and the refractive indices n_i of silver-adjacent layers ($i=L$ corresponds to a TiO_2 layer, $i=R$ to the active layer with $n_R=1.7$, see Figure 1). By eliminating the constant A, Eq. (1) is simplified and can be written in the factorized form

$$(1-(r_L r e^{2i\varphi_L})^{-1})(1-(r_R r e^{2i\varphi_R})^{-1}) = -t^2/r^2. \quad (2)$$

Equation (2) describes two coupled Tamm states, localized on either side of the metal film. The coupling between them is determined by the residual transmission t of the thin silver

layer. By using simplified expressions for the reflection coefficients, we can linearize Eq. (2). For metal, the coefficient reads

$$r^{TE,TM} \approx -\exp[2in_i\omega(1-\Theta_i^2/2n_i^2)/(\sqrt{\epsilon_b}\omega_p)], \quad (3)$$

where ω_P and ϵ_b are the metal plasma frequency (for silver $\hbar\omega_P = 3.74$ eV) and the background dielectric constant, respectively. The angle of light propagation Θ_i in the layers adjacent to silver (with respect to the surface normal) is assumed to be small. The simplified DBR reflection coefficients close to the Bragg frequency ω_0 with light incidence from layers with refractive index n_i are

$$r_{TE,TM} \approx \pm\exp[i(\beta_{TE,TM}(\omega-\omega_0))/\omega_0], \quad (4)$$

with $n_T = 2.1$ as the value of the high index DBR material TiO_2 and $n_S = 1.45$ for the low index layers of SiO_2 (negative sign for the case $n_T > n_S$). The Bragg frequency ω_0 is given by

$$\omega_0 = \frac{\pi c}{n_T d_T + n_S d_S}\left(1 + \frac{\Theta_i^2}{2}\frac{n_S d_T + n_T d_S}{n_T n_S}\right) \quad (5)$$

and

$$\beta_{TE,TM} = \frac{\pi n_T n_S}{n_i|n_T - n_S|}\left(1 \mp \frac{\Theta_i^2}{2}\frac{n_T^2 + n_S^2}{n_T^2 n_S^2}\right), \quad (6)$$

where the negative (positive) sign corresponds to TE (TM) polarization. The coupling strength is determined by the ratio t^2/r^2 and can be approximated by[23]

$$t^2/r^2 \approx \frac{4n_T^2\omega_0^2}{\omega_P^2 n_R^2 \cosh^2\left(d_m\sqrt{(\omega_P/c)^2 + k_x^2}\right)}, \quad (7)$$

where k_x denotes the in-plane wave vector and d_m is the silver layer thickness. After linearizing, Eq. (2) can be rewritten in the form of two coupled oscillators, $(\omega-\omega_A)(\omega-\omega_B) = \Omega^2$, with two solutions for ω (each having the same base Bragg frequency ω_0) $\omega_{1,2} = \omega_0 \pm \Omega$. At zero angle, the coupling constant reads

$$\Omega = \frac{2\sqrt{(n_T n_S + n_T(n_T + n_S))(n_T n_S + n_R(n_T + n_S))}}{n_T n_R \cosh^2\left(d_m\sqrt{(\omega_P/c)^2 + k_x^2}\right)}\frac{\omega_0^2}{\omega_P}. \quad (8)$$

The Tamm plasmon localized at the interface between the silver and the left DBR has a frequency different from the Bragg frequency ω_0 of the DBR for which the localization would be maximized. In order to tune the Tamm plasmon frequency to the DBR frequency ω_0, the thickness of the layer adjacent to the metal should differ from being quarter wavelength by $d = \pi c/(2\omega_0 n) - c/\omega_P$.

Furthermore, Eq. (6) shows that the difference between the phases for TE- and TM-polarized light is proportional to the square of Θ_i. Applying this analytical approach, we can obtain a fit of the split hybrid modes of a sample with a 40 nm silver layer inside our organic microcavity as shown in Figure 3(a). Additionally, in Figure 3(b), the parabolic dependence of the splitting on the incidence angle is shown.

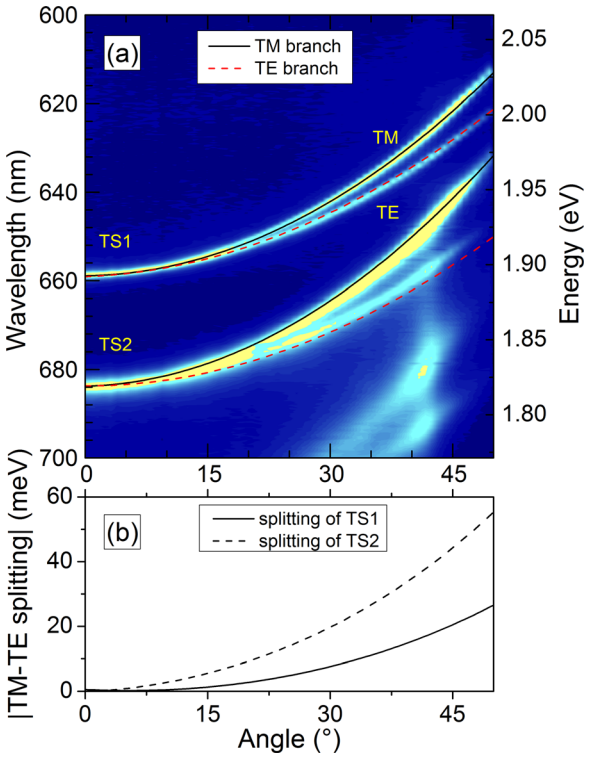

FIG. 3. (Color online) (a) For the special case of a 40 nm silver layer inside the cavity, analytical solutions (black solid and red dashed line) of the given analysis are presented showing good agreement with the experimental data. (b) Parabolic dependence of the splitting between TE- and TM-modes of the shifted cavity resonance and Tamm plasmon-polariton as a function of the angle of incidence.

In summary, the photon density of states of a microcavity changes substantially when a silver layer is embedded. The cavity mode is red-shifted due to coupling with the metal-based Tamm plasmon-polariton, and we are able to observe the associated spectral changes by using the emission spectrum of an organic semiconductor, which provides large oscillator strengths over a wide spectral range. The observed Tamm plasmon-polariton and the shifted cavity mode both exhibit parabolic dispersions $E(k)$. Depending on the detuning with respect to the DBR stop band, the dispersions of both modes split into orthogonally polarized (TE and TM) branches. We have presented an analytical model that explains the coupling between the two modes by the residual transmission of the metal layer. Excellent agreement with the experimental data is obtained. It turns out that the polarization splitting increases quadratically with increasing angle of incidence, again confirming the observations of the experiment. Thus, the coupling of Tamm plasmons and microcavity photons offers deep insights into the mode structure. Also, the ability to control the resonances of orthogonal polarization with such sharp spectral features is a very attractive property for optoelectronic device applications. Furthermore, the metal layer might also be used as an electrode enabling electrically driven thin and flexible displays and sensors.

We thank R. Scholz for useful discussions. The authors gratefully acknowledge financial support by the Deutsche

Forschungsgemeinschaft (DFG Project No. LE 747/37-1 and LE 747/41-1) and the European Commission (FP7 projects POLAPHEN and POLALAS (230811) and Clermont 4 (235114)) and RFBR.

[1]J. Kasprzak, M. Richard, S. Kundermann, A. Baas, P. Jeambrun, J. M. J. Keeling, F. M. Marchetti, M. H. Szymańska, R. André, J. L. Staehli *et al.*, Nature **443**, 409 (2006).
[2]R. Balili, V. Hartwell, D. Snoke, L. Pfeiffer, and K. West, Science (N.Y.) **316**, 1007 (2007).
[3]C. W. Lai, N. Y. Kim, S. Utsunomiya, G. Roumpos, H. Deng, M. D. Fraser, T. Byrnes, P. Recher, N. Kumada, T. Fujisawa *et al.*, Nature **450**, 529 (2007).
[4]A. Amo, J. Lefrère, S. Pigeon, C. Adrados, C. Ciuti, I. Carusotto, R. Houdré, E. Giacobino, and A. Bramati, Nat. Phys. **5**, 805 (2009).
[5]K. G. Lagoudakis, M. Wouters, M. Richard, A. Baas, I. Carusotto, R. André, L. S. Dang, and B. Deveaud-Plédran, Nat. Phys. **4**, 706 (2008).
[6]N. Gippius, I. Shelykh, D. Solnyshkov, S. Gavrilov, Y. Rubo, A. Kavokin, S. Tikhodeev, and G. Malpuech, Phys. Rev. Lett. **98**, 236401 (2007).
[7]I. Shelykh, T. Liew, and A. Kavokin, Phys. Rev. Lett. **100**, 116401 (2008).
[8]S. I. Tsintzos, N. T. Pelekanos, G. Konstantinidis, Z. Hatzopoulos, and P. G. Savvidis, Nature **453**, 372 (2008).
[9]D. Bajoni, A. Miard, A. Lemaître, S. Bouchoule, J. Bloch, and J. Tignon, Appl. Phys. Lett. **90**, 121114 (2007).
[10]T. C. H. Liew, A. V. Kavokin, and I. A. Shelykh, Phys. Rev. Lett. **101**, 016402 (2008).
[11]I. Shelykh, G. Malpuech, K. V. Kavokin, A. V. Kavokin, and P. Bigenwald, Phys. Rev. B **70**, 115301 (2004).
[12]F. Manni, K. G. Lagoudakis, T. K. Paraïso, R. Cerna, Y. Léger, T. C. H. Liew, I. Shelykh, A. V. Kavokin, F. Morier-Genoud, and B. Deveaud-Plédran, Phys. Rev. B **83**, 241307(R) (2011).
[13]M. Kaliteevski, I. Iorsh, S. Brand, R. A. Abram, J. M. Chamberlain, A. V. Kavokin, and I. A. Shelykh, Phys. Rev. B **76**, 165415 (2007).
[14]M. Kaliteevski, S. Brand, R. A. Abram, I. Iorsh, A. V. Kavokin, and I. A. Shelykh, Appl. Phys. Lett. **95**, 251108 (2009).
[15]T. C. H. Liew, A. V. Kavokin, T. Ostatnický, M. Kaliteevski, I. A. Shelykh, and R. A. Abram, Phys. Rev. B **82**, 033302 (2010).
[16]S. Reitzenstein, T. Heindel, C. Kistner, A. Rahimi-Iman, C. Schneider, S. Höfling, and A. Forchel, Appl. Phys. Lett. **93**, 061104 (2008).
[17]R. Brückner, M. Sudzius, S. Hintschich, H. Fröb, V. G. Lyssenko, and K. Leo, Phys. Rev. B **83**, 033405 (2011).
[18]G. Panzarini, L. Andreani, A. Armitage, D. Baxter, M. S. Skolnick, V. N. Astratov, J. S. Roberts, A. V. Kavokin, M. R. Vladimirova, and M. A. Kaliteevski, Phys. Rev. B **59**, 5082 (1999).
[19]F. Becker, M. Langner, H. Fröb, V. G. Lyssenko, K. Leo, and C. Adachi, Appl. Phys. Lett. **95**, 191106 (2009).
[20]E. Siebert-Henze, M. Langner, M. Sudzius, S. I. Hintschich, H. Fröb, V. G. Lyssenko, and K. Leo, Appl. Phys. Lett. **95**, 191116 (2009).
[21]S. Stelitano, S. Savasta, S. Patane, G. De Luca, and L. Monsù Scolaro, J. Appl. Phys. **106**, 033102 (2009).
[22]C. Sturm, H. Hilmer, B. Rheinländer, R. Schmidt-Grund, and M. Grundmann, Phys. Rev. B **83**, 205301 (2011).
[23]M. Born and E. Wolf, *Principles of Optics*, 7th ed. (Cambridge University Press, Cambridge, 1999).